Identification of intermetallic precipitates formed during re-solidification of brazed aluminium alloys

Moukrane Dehmas, Rocio Valdés, Marie-Christine Lafont, Jacques Lacaze and Bernard Viguier

CIRIMAT, ENSIACET-INP, UMR CNRS 5085, 118 route de Narbonne, 31077 Toulouse Cedex 4, France

This study shows that Fe and Mn bearing phases in Al–Si alloys containing a low level of Fe and Mn are essentially cubic α-Al(Fe, Mn)Si with Im3 space group and δ-AlFeSi which is observed with both tetragonal and orthorhombic structures. As this latter phase is not expected to form according to the ternary Al–Fe–Si phase diagram, the present results suggest that it is stabilized in the quaternary Al–Fe–Mn–Si system with respect to other phases such as β-Al_4FeSi.

Keywords: Aluminium alloys; Solidification; Intermetallic compounds; Electron diffraction

An analysis of the solidification sequence of some brazed aluminium clad alloys was presented previously [1] and [2]. The material consisted of a core made of AA3003 (essentially an Al–Mn alloy) clad on its two faces with AA4343. This latter alloy is an Al–Si alloy with some low level iron. During brazing, the assemblage is heated for a few minutes at a temperature where the overlay melts whilst the core material remains solid. Most of the liquid fills the joints between the various parts in contact but some remains on the flat surfaces. After brazing, both the joint and the re-solidified overlay were slightly enriched in Mn due to partial dissolution of the core material during the process. This enrichment leads to the formation of precipitates containing Al, Si, Mn and Fe in addition to the (Al) matrix and the silicon lamellae. In the joint, these precipitates were either blocky in a three-phase eutectic

with (Al) and silicon lamellae or Chinese-script in two-phase deposits with (Al) [1] and [2]. In the re-solidified overlay, the precipitates were again blocky in the three phase eutectics in the grain boundaries between the (Al) grains, or plate-like, when isolated inside or at the surface of the (Al) grains, as illustrated in Figure 1.

Figure 1. SEM micrograph of the surface of the re-solidified cladding (*SEI* detector, 15 kV, 32 mm, tilt 54°).

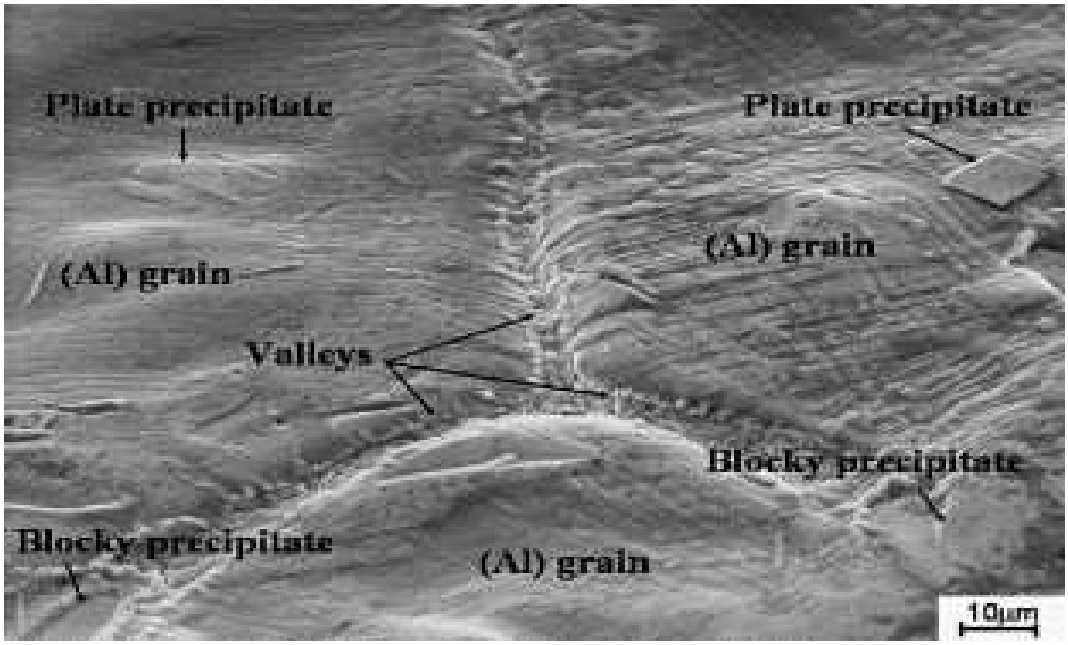

Energy dispersive X-ray (EDX) spectroscopy analyses performed in a scanning electron microscope (SEM) showed that both types of precipitates have similar silicon content, 10–12 at.%, with Mn and Fe apparently substituting for each other with a sum of their contents at 15–16 at.% [1] and [2]. By comparison to other literature data, these results suggested that these precipitates correspond to the cubic α-Al(Mn,Fe)Si phase most often designated as $Al_{15}(Fe,Mn)_3Si_2$ [3]. However, there is so much controversy in the literature concerning the structure and composition of the compounds appearing upon solidification of aluminium alloys containing Si, Mn and Fe [4] and [5], that it was decided to resort to transmission electron microscopy (TEM) examination coupled with EDX analysis to confirm the previous conclusion.

To prepare TEM samples, sheets of the flat surfaces of the brazed assemblages were polished down to a thickness of 150 μm while preserving intact one of the re-solidified surfaces. Disks with a diameter of 3 mm were then cut by a mechanical punch and the side opposite to the initial surface was gently dimpled before ion milling to transparency with a precision ion beam polishing machine (Gatan *PIPS*™). Ion polishing was done for a few hours until a hole had formed. During this step, the disk was observed periodically with an optical microscope to ensure that the hole was appropriately located. Figure 2 presents an optical micrograph of two of the thin foils thus prepared, where precipitates located near the hole have been indicated with arrows. All the observations reported below were made on these two samples which will be referred as samples 1 and 2. On the micrographs in Figure 2, the grain boundaries are easily recognized by their darker contrast. It is seen that the lower precipitate in sample 1 is located within an (Al) grain while the other precipitate as well as the one in sample 2 are within a grain boundary.

Figure 2. Optical micrographs of two TEM foils ((a) sample 1; (b) sample 2) prepared by ion milling showing the hole and precipitates located either in a grain boundary between (Al) grains or within an (Al) grain.

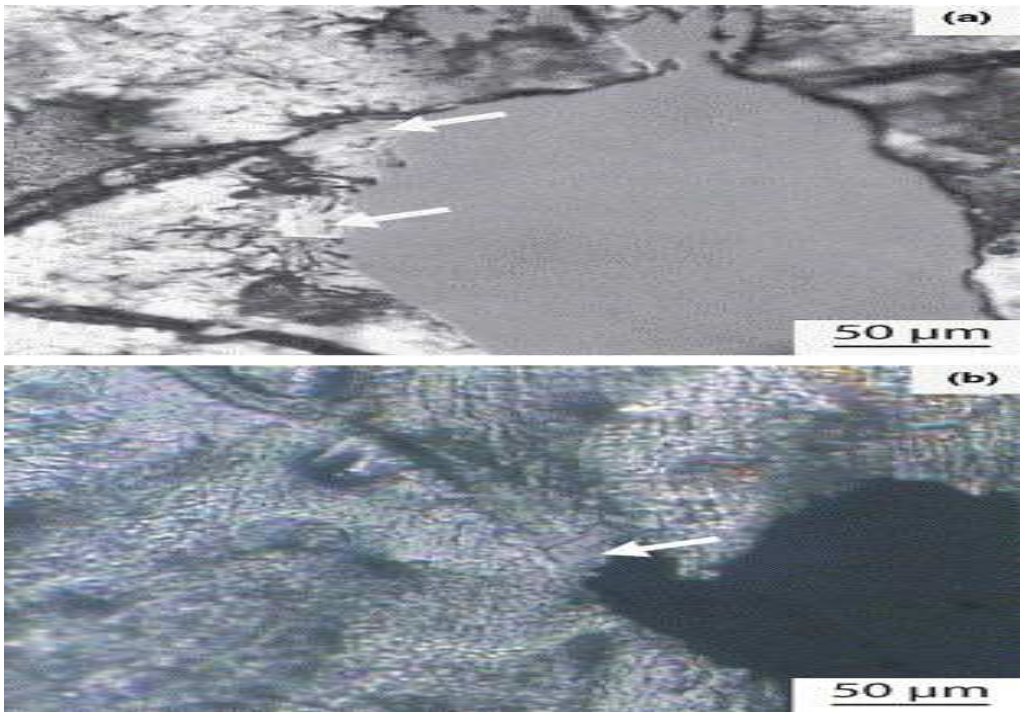

TEM investigations were carried out on a JEOL JEM-2010 operating at 200 kV and fitted with a double tilt specimen holder allowing tilts of ± 30° around two orthogonal axes. Chemical analyses were achieved by EDX spectroscopy coupled with the TEM, with a spot size of about 40 nm. The EDX spectra were recorded with an acquisition time of 60 s, and treated semi-quantitatively using the *k*-factor and including all usual corrections (absorption and fluorescence).

Figure 3 shows a TEM micrograph of each of the two precipitates of sample 1 identified in Figure 2. Figure 3(a) and (b) relate respectively to the precipitate in the (Al) grain and to the one in the grain boundary. The numbers on the micrographs refer to locations where EDX measurements were performed. The whole set of measured compositions is listed in Table 1.

Figure 3. Bright field images showing the two kinds of precipitates in sample 1: (a) precipitate in aluminium grain; (b) precipitate in the grain boundary.

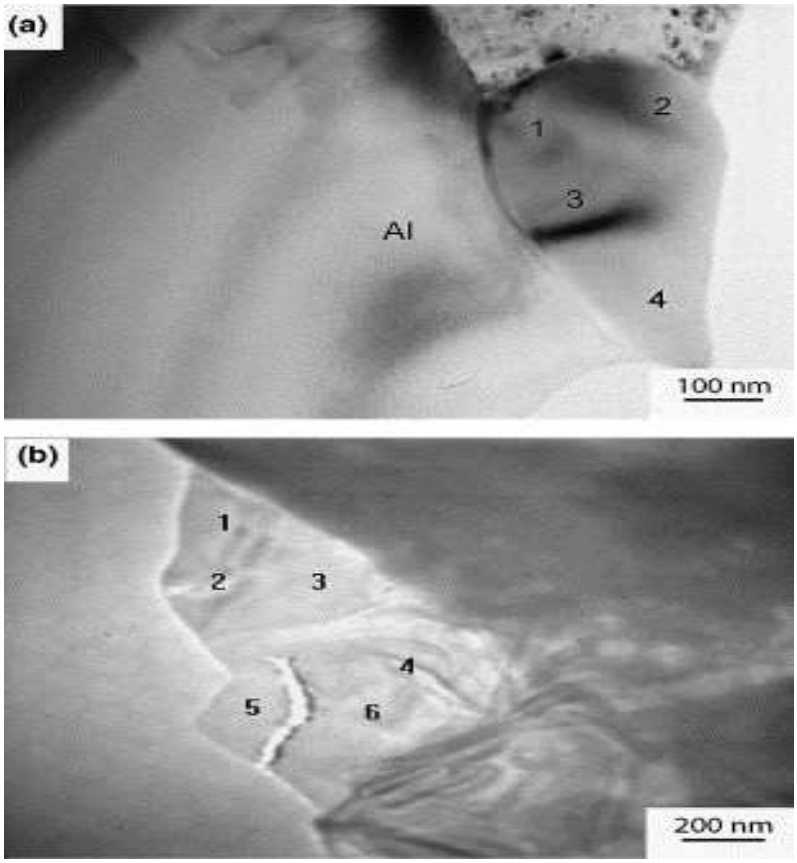

Table 1.

Compositions (at.%) measured by EDX in the TEM on the two precipitates in sample 1

	Precipitate in the (Al) grain				**Precipitate in the grain boundary**					
	1	**2**	**3**	**4**	**1**	**2**	**3**	**4**	**5**	**6**
Al	75	71	77.8	73.5	54	58.6	49	88	100	87
Si	10.5	10	10.2	9.7	35	29.8	42.5	8	–	8.2
Fe	10	14	8	12.3	8.5	9	6.5	3.5	–	3.7
Mn	4.6	4.2	4	4.5	2.3	2.6	2	0.7	–	0.8

The compositions measured on the precipitate in the (Al) grain are very similar to the values previously obtained by SEM–EDX [1] and [2]. They are in agreement with the composition of the α-Al(Fe,Mn)Si phase measured on as-cast alloys by various authors as reviewed previously [2], but also with measurements on heat-treated alloys [6], [7], [8] and [9]. Munson [10] showed that there is a family of quaternary α-AlFeMSi phases (with M being either V, Cr, Mo, W, Cu and Mn) having body-centred cubic (bcc) unit cells very similar to that of the simple cubic ternary α-AlMnSi phase. With increasing the Mn:Fe ratio, the bcc α-Al(Mn,Fe)Si phase would thus transform to the cubic α-AlMnSi phase. Cooper [11] investigated precipitates of this phase with a ratio Fe:Mn = 4:1 (corresponding to the formula $Al_{19}Fe_4MnSi_2$) and performed a refinement of its structure starting with the model of the α-AlMnSi phase which has a Pm3 space group [12].

Through this refinement, Cooper showed that the α-Al(Fe,Mn)Si has an Im3 space group [11], and this has been found by other authors since then [13]. Donnadieu et al. [14] investigated further the Im3 and Pm3 structures through TEM analysis of precipitates in 6xxx aluminium alloys, and showed that there is a transition between the two structures which depends on the Mn:Fe ratio in the intermetallic phase. However, to the best knowledge of the authors, no information is available on the type of transition involved.

Electron diffraction patterns along the [1 1 1] and [2 3 0] zone axes recorded for the precipitate shown in Figure 3(a) are reproduced in Figure 4(a) and (b), respectively. Also, diffraction patterns for the Im3 and Pm3 structures were simulated using the EMS software [15] and are also shown in Figure 4. The calculations were performed with the description of

the phases given by Cooper [11]. It is seen that along the [1 1 1] zone axis, the extinctions are similar for both space groups, while along the [2 3 0] zone axis, the reflections for which $h + k + l$ is odd appear for the Pm3 group and not for the Im3 one. From this, it is concluded that the α-Al(Fe,Mn)Si phase observed in this study is cubic with the Im3 space group with a unit cell parameter close to 12.5 Å. This result agrees with the previous study by Donnadieu et al. [14] as the Mn:Fe ratio of the observed precipitate is quite low at 0.4 (Table 1).

Figure 4. Experimental selected area diffraction patterns (SAD) of the precipitate located in the (Al) grain (Figs. 2(a) and 3(a) for the [1 1 1] (a) and [2 3 0] (b) zone axes, and simulation of the pattern expected at these orientations for Im3 (c), (d) and Pm3 (e), (f) space groups.

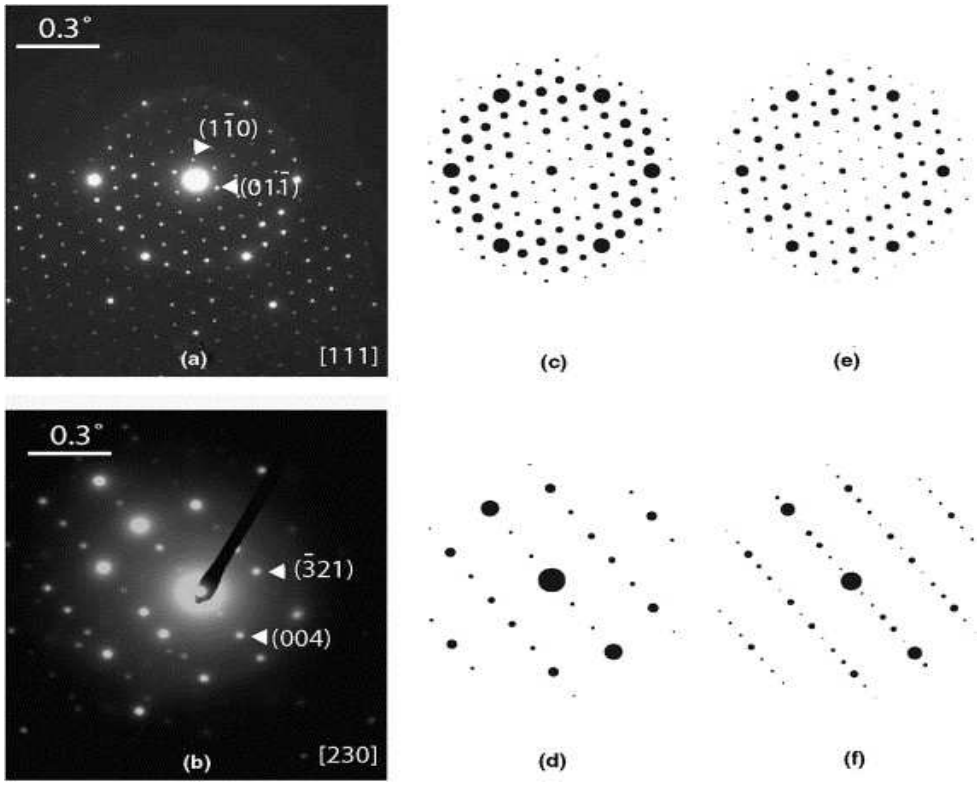

Concerning the precipitate in the grain boundary, it is seen in Table 1 that the measurements may be sorted into two classes—compositions showing either high silicon content (30–42.5 at.%) or high aluminium content (more than 87 at.%). These latter values are most likely due to a contribution of the aluminium matrix and will not be considered further. Looking at

the various compounds appearing in the Al–Fe–Si system, it was found that this high silicon content may fit with the composition of the Al_3FeSi_2 phase (Fe 15–17 at.%, Si 27–43 at.%, Al 40–58 at.%) as reviewed by Gueneau et al. [16]. This phase is most often called δ-AlFeSi.

The structure of the phase Al_3FeSi_2 has been reported as being either orthorhombic [16] or tetragonal [13], [17] and [18] with nearly the same unit cell parameters. The orthorhombic structure may be distinguished from the tetragonal one by the presence of superstructure reflections, though there are only few zone axes allowing effectively such a distinction to be made, e.g. the [2 1 0] zone axis. Another methodology that was used in the present work to remove the uncertainty is based on the analysis of features of the reflection nets in the diffraction patterns including zero-order Laue zone (ZOLZ), first-order Laue zone (FOLZ) and second-order Laue zone (SOLZ). Simulation of diffraction patterns including high-order Laue zones (HOLZ) was performed by using the EMS program and the structural data obtained by Panday et al. [17] for the tetragonal structure and by Gueneau et al. [16] for the orthorhombic one. The relative intensity of spots from HOLZ has been arbitrarily increased in order to enhance the visual representation of the simulated patterns and the maximum deviation parameter from the Bragg position $(s_g^{\max})$ has been fitted to get the right number of spots in the ZOLZ. The identification of the structure was performed on a series of conventional selected area electron diffraction patterns (SAD) of different orientations with large angular separations recorded from the same area of the particle. Figure 5 presents the experimental diffraction pattern along the [1 3 5] zone axis (a) and the corresponding calculated patterns according to the tetragonal (b) and orthorhombic (c) unit cells. The comparison between the two simulated patterns reveals the absence of reflections in the FOLZ for the tetragonal structure in contrast to the orthorhombic structure. Comparison with the experimental SAD pattern shows that the structure is tetragonal with the I4/mcm space group (a = 6.1 Å; c = 9.5 Å), and the other electron diffraction patterns recorded on this precipitate were easily indexed considering a tetragonal unit cell.

Figure 5. Experimental electron diffraction patterns for the precipitate in the grain boundary of sample 1 along the [1 3 5] zone axis (a) and corresponding calculated patterns according to a tetragonal (b) and orthorhombic unit cell (c) for $s_g^{\max} = 0.1\ \mathrm{nm}^{-1}$ (solid disks: ZOLZ; empty circles: FOLZ; crosses: SOLZ).

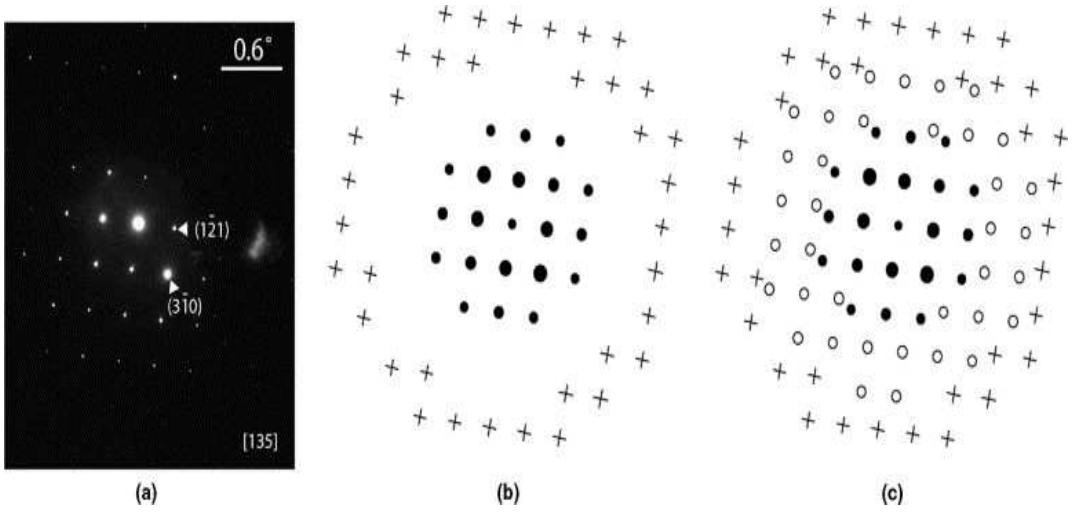

Figure 6 shows a bright field image of the precipitate in sample 2 (Fig. 2(b)) that is also located in a grain boundary. EDX measurements were performed in various locations indicated with numbers on the figure and are reported in Table 2. The compositions obtained could be sorted in two groups, one rich in silicon (23–37 at.% Si) expected to correspond to the Al_3FeSi_2 phase as above and the other lower in silicon (7.1–17 at.% Si) that could correspond to the Al_4FeSi phase [18]. Attention was focused only in the present work on the areas with high silicon content. Figure 7 shows the experimental pattern along the $[3\bar{1}5]$zone axis (a) and the simulated patterns corresponding to the tetragonal (b) and orthorhombic (c) structures. It is seen that reflections in the first-order Laue zone are consistent with an orthorhombic structure (Pbcn space group), with unit cell parameters: a = 6.1 Å and c = 9.5 Å. Weak additional spots in the ZOLZ can easily be explained by double diffraction phenomena that may occur between the different Laue zones.

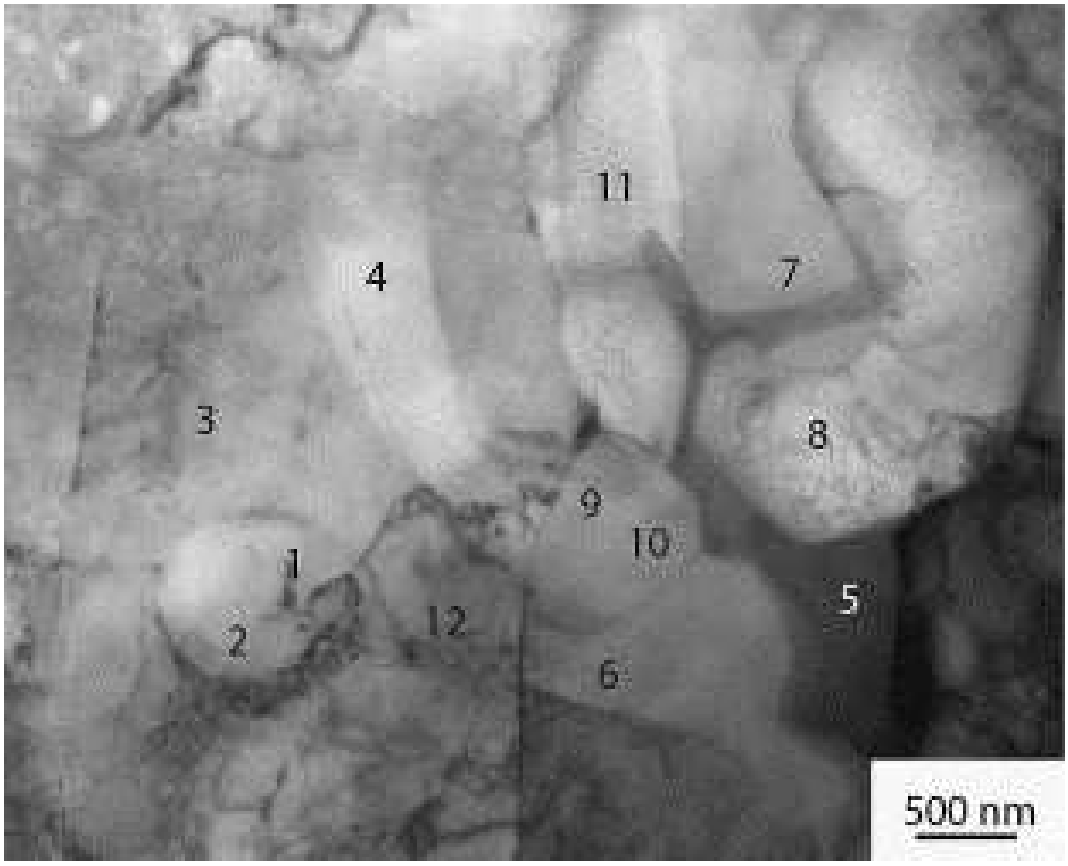

Figure 6. Bright field image of the precipitate in the grain boundary of sample 2. The numbers refer to locations of EDX measurements.

Table 2.

Compositions (at.%) measured by EDX in the TEM on the precipitate in sample 2

	1	**2**	**3**	**4**	**5**	**6**	**7**	**8**	**9**	**10**	**11**	**12**
Al	76.5	58.9	79.8	76.8	71.0	66.0	70.9	57.4	83.2	58.9	78.8	88.0
Si	17.0	35.1	12.8	15.9	24.0	28.0	23.1	37.1	10.3	35.1	13.8	7.1
Fe	4.6	4.21	5.1	5.0	4.0	4.6	4.2	3.9	4.5	4.2	5.1	3.5
Mn	1.9	1.71	2.2	2.1	1.5	1.9	1.7	1.5	1.8	1.7	2.1	1.4

Figure 7. Experimental electron diffraction patterns for the precipitate in the grain boundary of sample 2 along the $[3\,\bar{1}\,5]$zone axis (a) and corresponding calculated pattern indexed according to the tetragonal (b) and orthorhombic (c) unit cells for $s_g^{max} = 0.07\ nm^{-1}$(solid disks: ZOLZ; empty circles: FOLZ; crosses: SOLZ).

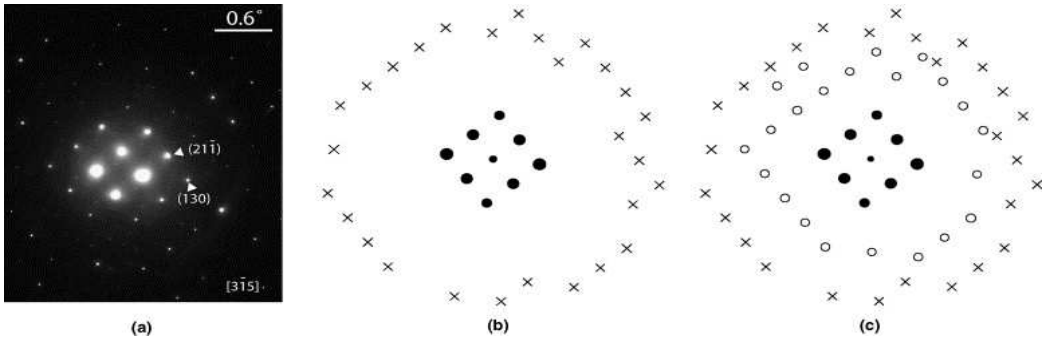

The present study showed, in agreement with recent work [4], that the Fe and Mn bearing phases in Al–Si alloys containing low level of Fe and Mn are essentially cubic α-Al(Fe,Mn)Si with the Im3 space group and δ-AlFeSi. This latter phase was found with both tetragonal and orthorhombic structures in the same sample. This phase appears in the ternary Al–Fe–Si diagram and has a composition most often referred to as Al_3FeSi_2, but would better be written as $Al_3(Fe,Mn)Si_2$ when dealing with alloys containing both Fe and Mn. As there is no equilibrium between the (Al) and δ-AlFeSi phases in the ternary Al–Fe–Si phase diagram, the formation of this latter phase rather than the Al_4FeSi phase upon solidification of Al–Si alloys should be investigated further. The present study suggests this is due to a stabilization of the $Al_3(Fe,Mn)Si_2$ phase with respect to the β-Al_4FeSi phase in the quaternary Al–Fe–Mn–Si system.

References

S. Tierce, N. Pébère, C. Blanc, G. Mankowski, H. Robidou, D. Vaumousse and J. Lacaze, *Int. Cast Met. Res. J.* 18 (2005), p. 370.

J. Lacaze, S. Tierce, M.-C. Lafont, Y. Thebault, N. Pébère, G. Mankowski, C. Blanc, H. Robidou, D. Vaumousse and D. Daloz, *Mater. Sci. Eng. A* 413–414 (2005), p. 317.

L.F. Mondolfo, Aluminium alloys: structure and properties, Butterworth, London (1976).

M.V. Kral, *Mater. Lett.* 59 (2005), p. 2271.

A.M. Zakharov, I.T. Guldin, A.A. Arnold and Y.A. Matsenko, *Russ. Metall.* 4 (1989), p. 209.

M. Dehmas, P. Archambault, M. Serriere, E. Gautier and C.-A. Gandin, *Aluminium* 80 (2004), p. 619.

Y. Li and L. Arnberg, *Acta Mater.* 51 (2003), p. 3415.

E. Tromborg, A.L. Dons, L. Arnbergm, Aluminium alloys, in: proceedings of ICAA3, Mater. Sci. Forum 1992, 285.

P. Furrer and G. Hausch, *Met. Sci.* 13 (1979), p. 155.

D. Munson, *J. Inst. Met.* 95 (1967), p. 384.

M. Cooper, *Acta Cryst.* 23 (1967), p. 1106.

M. Cooper and K. Robinson, *Acta Cryst.* 20 (1966), p. 614.

M.V. Kral, H.R. McIntyre and M.J. Smillie, *Scripta Mater.* 51 (2004), p. 215.

P. Donnadieu, G. Lapasset and T.H. Sanders, *Philos. Mag. Lett.* 70 (1994), p. 319.

P. Stadelmann, *Ultramicroscopy* 21 (1987), p. 131.

C. Gueneau, C. Servant, F. d'Yvoire and N. Rodier, *Acta Cryst.* C51 (1995), p. 177.

P.K. Panday and K. Schubert, *J. Less-Common Met.* 18 (1969), p. 175.

V.G. Rivlin and G.V. Raynor, *Int. Met. Rev.* 3 (1981), p. 133.

Corresponding author. Tel.: +33 5 62 88 56 53; fax: +33 5 62 88 56 63.